REVIEW ARTICLE

Review of plane grating focusing for soft x-ray monochromators

H. Petersen, C. Jung, C. Hellwig, W. B. Peatman, and W. Gudat
BESSY GmbH, Lentzeallee 100, D-14195 Berlin, Germany

(Received 6 June 1994; accepted for publication 26 September 1994)

During the last 10 years various types of soft x-ray monochromators have been developed, which are optically based on the plane grating focusing condition introduced in 1980. These instruments as well as those using the original 1980 optical configuration are reviewed and compared to the other type of high performance soft x-ray grating monochromator, the Rowland circle based spherical grating monochromator (SGM). Performance data of a plane grating monochromator (HE-PGM-3), which was recently commissioned at BESSY and which offers a broad spectral range (40–2000 eV) and very high spectral resolution (up to $E/\Delta E \sim 10\,000$) are given in more detail. The performance of grating and crystal monochromators is compared in the 1–2 keV photon energy range. © *1995 American Institute of Physics.*

I. INTRODUCTION

Science with soft x-rays has boomed over the last decade and is still strongly expanding.[1] There are mainly two reasons: (1) synchrotron radiation sources of the second and third generation[2] provide intense soft x-rays from undulator sources and (2) high performance monochromators, some of which will be discussed in this review, provide small photon energy bandwidths to make high spectral resolution research possible. For general references see the proceedings of various national and international conferences on synchrotron radiation instrumentation.[3] In this paper we will restrict ourselves to monochromators optimized for the 40–2000 eV range.

The first milestone regarding very high spectral resolution in the soft x-ray range was made on a spherical grating monochromator (SGM) at the NSLS in Brookhaven in 1988.[4,5] It has opened up completely new fields of research. In the meantime various other very high resolution soft x-ray monochromators have been put into operation, some similar to the NSLS-SGM and some optically different.[6–13] In this article we review one category of the latter, namely those using plane gratings and applying the plane grating focusing condition.[14] These instruments provide very high spectral resolution over a continuous broad photon energy range requiring only a single diffraction grating.

Soft x-ray monochromators have always been known to be technologically extremely demanding for the following simple reasons. There are two conflicting goals: to minimize optical aberrations one would like to employ normal incidence optics; but to obtain a reasonable reflectivity, one has to go to grazing incidence on the optical elements. Also, to achieve very high resolution of ~10 000 one has to isolate an extremely small wavelength band of typically 0.0002 nm, a resolution of ~3 million in the visible. The grating constant is typically 833.33 nm (standard 1200 lines/mm grating) i.e., more than for 4 million times larger than the desired wavelength resolution. At BESSY, for example, we work with a 10 μm exit slit 5 m beyond the diffraction grating in order to isolate the angular interval corresponding to such a wavelength band.

Because of the facts given above, excellent optical solutions and extreme technological quality in both optics and kinematics are obviously necessary for soft x-ray grating monochromators if one wants to achieve high resolution.

Spherical grating monochromators combine the dispersive characteristics of a grating with the first order focusing characteristics of a spherical surface. The well-known Rowland circle spherical grating optical solution[15] has been used in the first monochromator which provided useful photon flux and resolution in the soft x-ray range above the carbon K-edge (282 eV), namely the so-called "Grasshopper".[16] The very successful NSLS-SGM "Dragon" can also be operated in the Rowland mode over a limited part of its operational range.[4,5] In Fig. 1(a) we show the Rowland circle geometry and in Figs. 1(b) and 1(c) the optical schemes of both the "Grasshopper" and the "Dragon" monochromators. Although the Rowland circle looks simple, instrumental geometry becomes rather complicated, as soon as the requirements of fixed input direction (and slit if possible) and fixed exit direction (and slit if possible) are introduced, as it is the most desired case at synchrotron radiation facilities.

Plane gratings as diffraction elements have quite a long history, starting with Ebert's work in 1889 [see, e.g., Refs. 17–20]. In the early cases[17–19] they were associated with parallel light, probably, because at first glance plane gratings seemed to have no focusing properties at all. The nonparallel-light case was explicitly discussed in 1949 and 1962.[21,22] Figure 2 shows the focal curves of a plane grating in divergent light, using various fixed grazing incidence angles α as a parameter. These curves are lemniscates, and were first published by Murty in 1962.[22] At first glance, these curves do not look very promising as far as the realization of a simple perfect focusing geometry is concerned. The situation did, however, change considerably when the plane grating focusing condition was introduced in 1980.[14] This will be further discussed below.

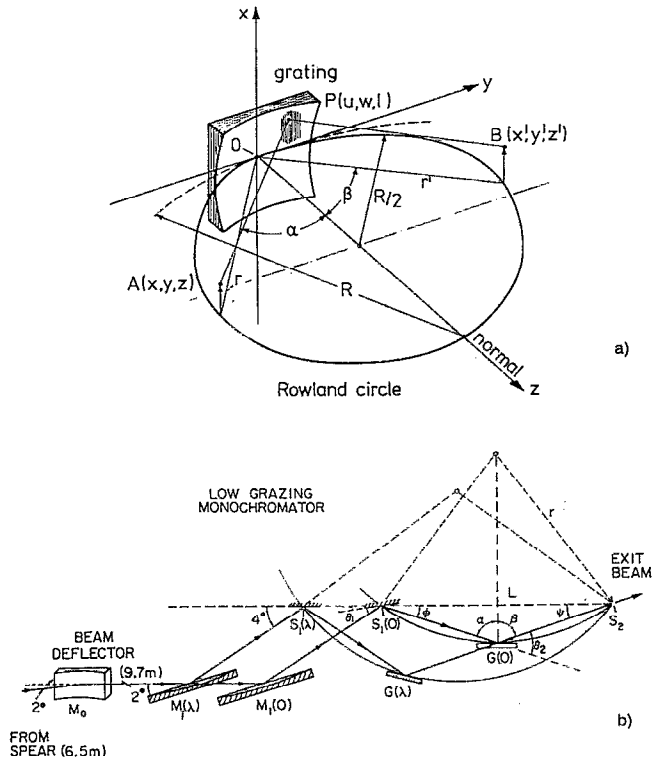

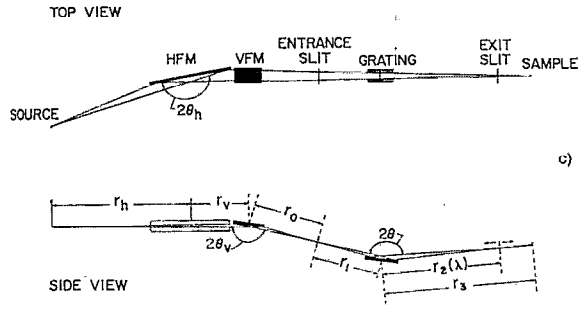

FIG. 1. (a) The Rowland circle geometry. Note, for our development we use the grazing angles of incidence and diffraction. (b) The optical configuration of the first efficient soft x-ray monochromator, the so-called "Grasshopper" (from Ref. 16). (c) The optical configuration of the first high resolution soft x-ray monochromator, the so-called "Dragon"-SGM (from Ref. 4).

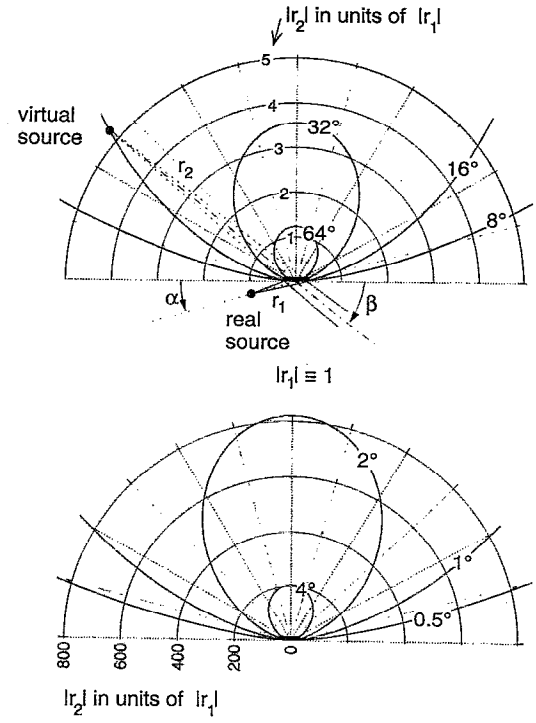

FIG. 2. Focal curves for a plane grating in divergent light. The virtual source distances r_2 are given in units of the real source distance r_1 as a function of the grazing incidence angle α as a parameter. These curves are lemniscates, $r_2 = -r_1(\sin\beta/\sin\alpha)^2$. For $\alpha=16°$ the position of the virtual source and the outgoing light beam are given for a fix-focus constant $c_{ff}=2.25$.

Arguments are, of course, slightly different for crystal monochromators, but these are not really competitive in the photon energy range below 1000 eV. The only crystal with an adequate d spacing for that energy range, namely beryl, is not very radiation resistant and must be replaced quite often—very different from gratings. Crystal monochromators are clearly superior to grating instrumentation only when silicon crystals can be used, i.e., above ~2000 eV, as we will see later.

II. PLANE GRATING MONOCHROMATORS: THEORY AND PERFORMANCE

In this section we will chronologically describe the development of focusing plane grating monochromators since 1980. Performances will be illustrated by typical examples of experimental data. As much of the present research uses circularly polarized soft x-rays, we will discuss the transfer function of PGMs for polarized SR. Finally, the most recently commissioned focusing PGM, the so-called BESSY HE-PGM-3, will be presented in more detail.

Based on Kunz's well-known plane grating/sliding mirror monochromator GLEISPIEMO[20,23] soft x-ray plane grating instrumentation was further developed at BESSY. This led to a considerable extension of the spectral range covered, and to the introduction of the plane grating focusing condition $\sin\beta/\sin\alpha$=const=fix-focus-constant "c_{ff}". The upper two optical schemes of Fig. 3 illustrate this step. Note that we have employed the grazing angles of incidence and diffraction.

Deducing the virtual source position, r_2, from the grating focusing equation

$$\frac{\sin^2\alpha}{r_1}-\frac{\sin\alpha}{R}+\frac{\sin^2\beta}{r_2}-\frac{\sin\beta}{R}=0, \tag{1}$$

with $R\to\infty$ (plane grating case) we have

$$r_2=-r_1\left(\frac{\sin\beta}{\sin\alpha}\right)^2. \tag{2}$$

Under the plane grating focusing condition[14] the ratio $\sin\beta/\sin\alpha$ is kept constant leading to exact focusing with fixed entrance and exit armlengths, i.e.,

$$r_2=-r_1\cdot c_{ff}^2. \tag{3}$$

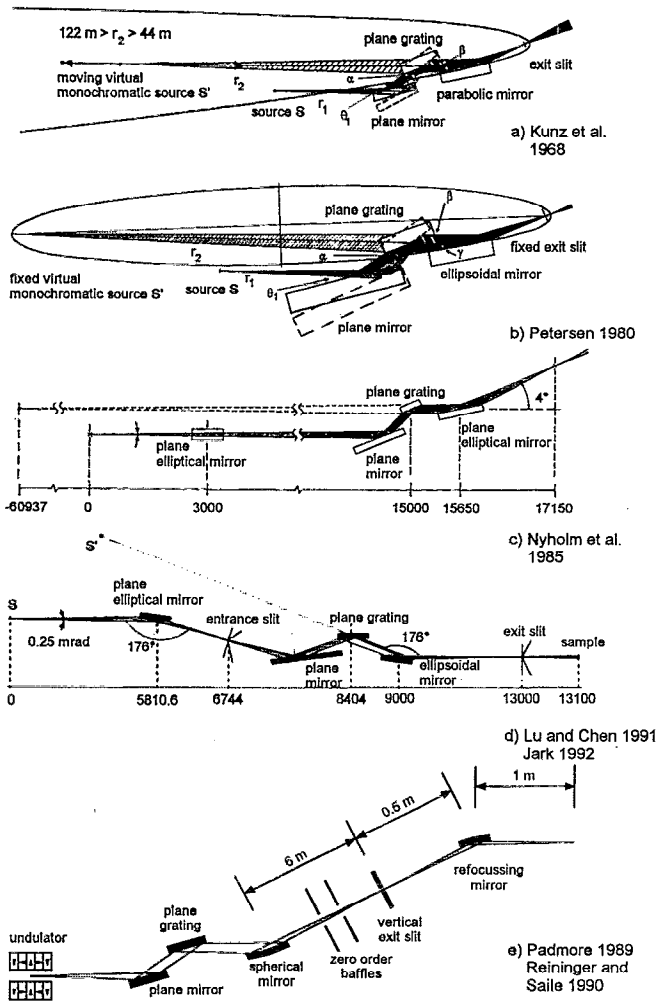

FIG. 3. The introduction of the plane grating focusing condition and optical designs using it (as of September 1994); (a) The Kunz' GLEISPIEMO (Refs. 20 and 23) drawn in a style similar to (b). (b) The introduction of the plane grating focusing condition; Kunz' parabolic mirror is replaced by an ellipsoidal one. (c) Two plane-elliptical mirrors: Nyholm *et al.* (Ref. 37). (d) Preoptics, entrance slit, stigmatic layout: Lu and Chen (Ref. 40), Jark (Ref. 41). (e) Spherical mirror: Padmore (Ref. 42), Reininger and Saile (Ref. 43).

Together with the grating equation

$$n \cdot \lambda = d(\cos \alpha - \cos \beta) \tag{4}$$

the angles α and β are determined for a given photon energy and a given c_{ff} constant. In the diagram of Fig. 2 the virtual source then rotates on a circle. The tunable virtual monochromatic source can be fixed in space, when the grating and the direction of the incoming light beam are both rotated around the axis in the center of the grating according to the plane grating focusing condition. The fixed virtual source has to be imaged into real space onto the fixed exit slit by some focusing element.

In the 1980 version of the optics, the fixed virtual source was imaged by a rotationally symmetric ellipsoidal mirror onto the fixed exit slit [compare Fig. 3(b)]. The first instrument with the new optics, the Zeiss-built SX700/1 monochromator,[14,24,25] was delivered in late 1982 and has now been in successful operation for more than ten

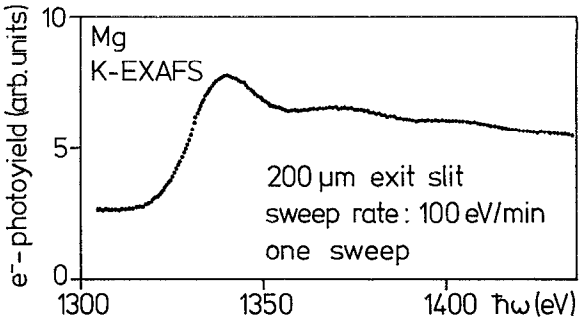

FIG. 4. Mg K-photoyield-EXAFS spectrum measured at the SX700/1 using a 610 lines/mm mechanically ruled grating. Data are not normalized or treated otherwise (from Ref. 26).

years.[26–28] The instrument includes a kinematically simple solution for the rotation of the incoming light beam around the axis of grating rotation.[24,25] In Fig. 4 we show the Mg K-EXAFS spectrum, which was obtained immediately after delivery using a mechanically ruled 610 lines/mm grating.[27] No normalization or any other kind of data treatment has been applied. Note the high spectral purity: the signal below the K edge, which is mainly due to stray light induced photoemission, is small compared to the edge jump. To illustrate the continuous broad photon energy range a gold photoyield spectrum measured in 1984 with an ion etched 1221 lines/mm grating is given in Fig. 5.[28] For the conversion into photon flux at 700 eV the gold quantum yield data of Ref. 29 were used, the bandwidth at 700 eV was about 1.7 eV. In the meantime fourteen such PGMs using the plane grating focusing condition, among them nine SX700s, are in service at various laboratories (see Table I).

After the ellipsoidal focusing mirrors had reached the target specification of 0.5 arcsec rms tangent error over the whole mirror surface in 1990, very high spectral resolution has been obtained at BESSY with this specific type of optics.[11,30] However, for best values the ellipsoidal mirror has still to be shadowed off to a small fraction of its surface because of remaining tangent errors. This was, for example,

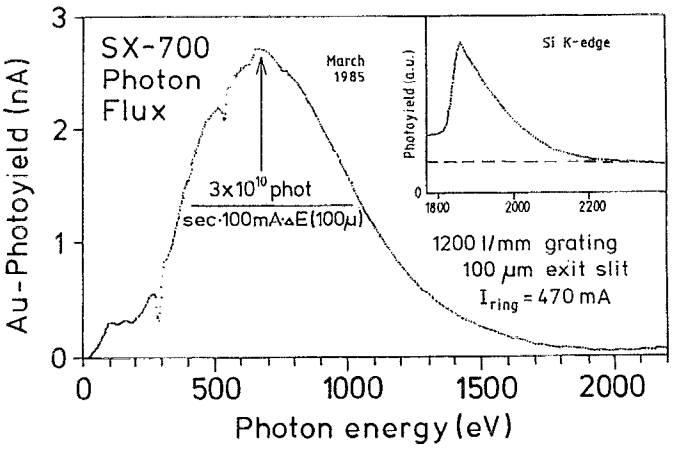

FIG. 5. Gold-photoyield spectrum measured at the SX700/1 using a 1221 lines/mm ion etched grating. To emphasize the spectral purity the Si K-edge is included (from Ref. 28).

TABLE I. Monochromators based on the plane grating focusing condition (as of September 1994).

Location	Type	Focusing	Dipole/ insert.dev.	References
Berliner Elektronen-speicherring-Gesellschaft für Synchrotronstrahlung (BESSY), Berlin	SX700/1	ellipsoid	dip	14,24,28
	SX700/2/FUB	ellipsoid	dip	11,14,24,30
	SX700/3	ellipsoid	dip, circular	14,24,32
	HE-PGM-2	ellipsoid	dip	14,28
	HE-PGM-3	2 spheres	dip	12,14,42,43,44
	SX700/PTB	ellipsoid	dip	14,24,52
Center for Advanced Microstructures and Devices (CAMD), Baton Rouge, LA	CAMD-PGM	sphere entrance slit	dip	14,43,69,70
Hamburger Synchrotronstrahlungs-labor (HASYLAB), Hamburg	SX700	sphere	triple undulator	13,14,24,43,45,46
Instrument Center for Synchrotron Radiation (ISA), Aarhus	SX700	ellipsoid	dip	14,24
MAX-LAB Lund	SX700	two plane	dip	14,24,37
	SX700	ellipsoids	undulator	14,24,37,71
Synchrotron Radiation Center (SRC), Wisconsin	Aladdin-PGM	ellipsoid entrance slit	undulator	14,40,41
Synchrotron Radiation Source (SRS), Daresbury	Stat. 5U.1	sphere	undulator	14,42,72
ELETTRA Trieste	SX700	ellipsoid entrance slit	undulator	14,24,41

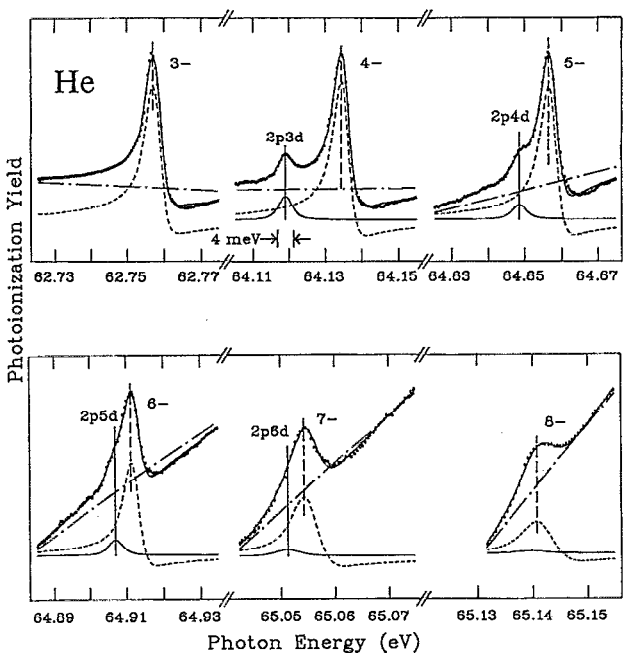

FIG. 6. $(sp,2n^-)^1P^0$ and $(2p,nd)^1P^0$ resonances of doubly excited helium taken at the SX700/2. This was the first experimental observation of the $(2p,nd)^1P^0$ series (from Ref. 31).

necessary during the first observation of the $(2p,nd)^1P^\circ$ double excitation Rydberg series of helium, which was found by Domke *et al.* using a bandpass of 4 meV at 64 eV photon energy (see Fig. 6).[31]

One of the PGMs at BESSY, the SX700/3, is installed in such a way that it accepts the circularly polarized synchrotron radiation from above or alternatively from below the plane of the storage ring.[32] For this purpose two plane mirrors under 2° grazing incidence in *s*-reflection are mounted in front of the monochromator. In the dipole SR-source case of completely polarized light with a phase difference of 90° between $I_\parallel$ and $I_\perp$ the degree of circular polarization is given by

$$P_{\text{circ}}(h\nu,\psi)=|S_3|=2\cdot\frac{\sqrt{I_\parallel I_\perp}}{I_\parallel+I_\perp}. \tag{5}$$

S_3 is one of the Stokes parameters. P_{circ} is largely conserved in the SX700/3, because the instrument is always operated at grazing angles, even for low photon energies like 30 eV. The angular range around 45° incidence angle, where the 90° phase relation between the horizontally and vertically polarized radiation from the dipole source is destroyed by the strongly phase shifting optics, is thus completely avoided. Figure 7 shows a circular polarization map of the SX700/3-beamline. Values of P_{circ} on the researchers sample are given as a function of both the photon energy and the off-plane

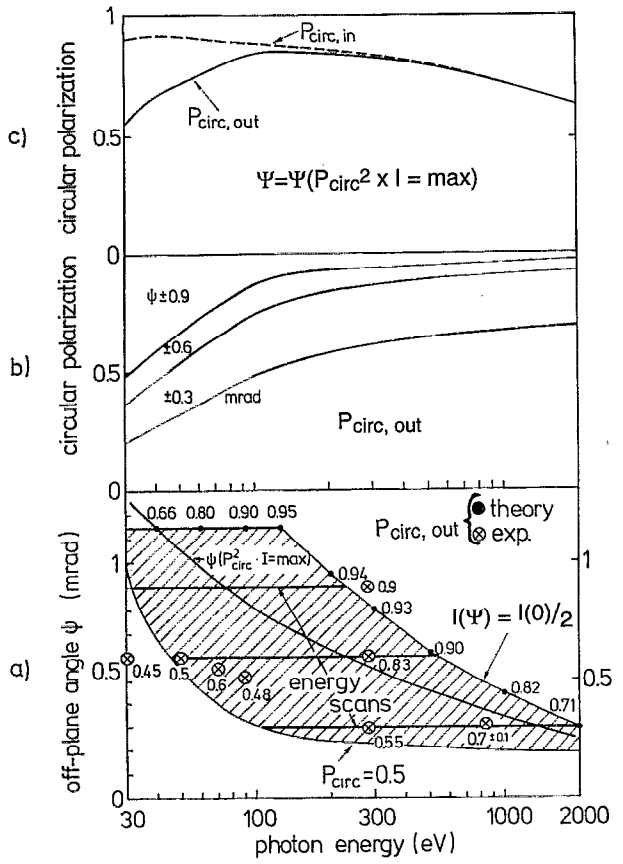

FIG. 7. (a) Circular polarization map of the SX700/3: Above the hatched area the values of P_{circ} and $I(h\nu,\psi)/I(h\nu,0)$ are larger than 0.5 (calculation). The product $P^2_{circ}I$ is maximal above the $\psi(P^2_{circ}I=\max)$-curve. Included are the three energy-scan-ranges for constant ψ and experimental data, see text for details. (b) P_{circ} on the sample calculated for the three energy-scan-values ψ=0.3, 0.6, 0.9 mrad; outside the recommended energy ranges the lines are drawn thinner. (c) P_{circ} above the $\psi(P^2_{circ}I=\max)$-curve, as emitted by the dipole magnet ($P_{circ,in}$) and on the sample ($P_{circ,out}$). Note the small depolarization effects (from Ref. 32).

angle ψ in the lower part. Experimental data as measured with a polarimeter using mirror optics ($h\nu$=30, 50, 70, 90 eV)[32,33] and using multilayer optics ($h\nu$=265 eV)[34] and estimated from photoemission data ($h\nu$=700 eV)[35] are included. The values of P_{circ} along the photon-energy scan lines are given in the middle part, and the curve for P_{circ} as emitted by the dipole magnet and as available at the sample is plotted in the top part; the ψ values selected for this curve are those which give the highest values in the figure-of-merit product

$$P^2_{circ}(h\nu,\psi)\cdot I(h\nu,\psi)=\left(2\cdot\frac{\sqrt{I_\parallel I_\perp}}{I_\parallel+I_\perp}\right)^2\cdot(I_\parallel+I_\perp)$$
$$=4\cdot\frac{I_\parallel I_\perp}{I_\parallel+I_\perp}, \qquad (6)$$

where $I(h\nu,\psi)$ is the photon flux at the elevation angle ψ.

This circular-soft-x-ray beamline is now very popular at BESSY and many new scientific results have been obtained on it, among them soft x-ray microscopy pictures of magnetic domains using a fast parallel-imaging electron analyzer (see Fig. 8[36]).

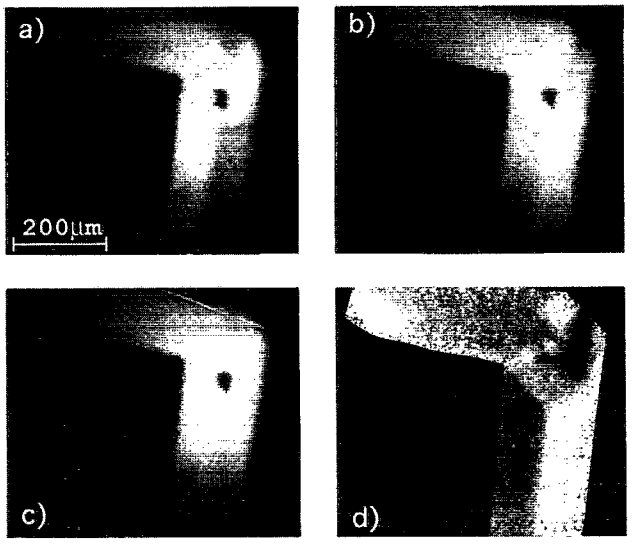

FIG. 8. Spectromicroscopy from iron whisker using L_3VV Auger electrons at the SX700/3. The images have been recorded with right-hand circularly polarized light of 708 eV (a) and 720 eV photon energy (b), the light being incident under 25° to the surface of the whisker. The sum (c) and the normalized difference (d) of the raw images show the topography (c), and the magnetic contribution (d) to the total contrast. Dark (white) areas in (d) represent domains with a magnetization vector upwards (downwards) along the vertical axis (from Ref. 36).

We will now describe some optical configurations which use the plane grating focusing condition but are otherwise different from the 1980 version of the optics discussed above.

The necessity to close down the aperture because of existing tangent errors on the ellipsoidal mirror has been mentioned. Another reason for closing down the aperture for very high resolution is the astigmatism of the optics. The astigmatism gives rise to an astigmatic coma aberration from the ellipsoidal mirror, which increases quadratically with sagittal aperture, as shown in the ray tracing Fig. 9(a). In 1985 Nyholm *et al.*[37] addressed this point and suggested decoupling meridional and sagittal focusing using two plane elliptical mirrors for this purpose [Fig. 3(c)]. With these optics, the light spot on the sample can be tailor-made to the researchers needs, because focal spot distance and magnification in the sagittal direction can be selected independently. The raytracing is shown in Fig. 9(b). At Maxlab one decided to use the modified SX700 for high resolution photoemission spectroscopy and very successful work was done.[38] As an example Fig. 10 shows the contributions of the surface atoms in an electron energy distribution curve for two geometrically different rhodium surfaces.[39] In Fig. 9(c) we calculated this optical configuration in a slightly different version, which is preferable if a very small spot at the exit slit has to be created, for example, for photoelectron microscopy applications.

Another elegant way to eliminate astigmatism was found by Lu and Chen[40] and by Jark:[41] an entrance slit was introduced and positioned such that the distances real-source to

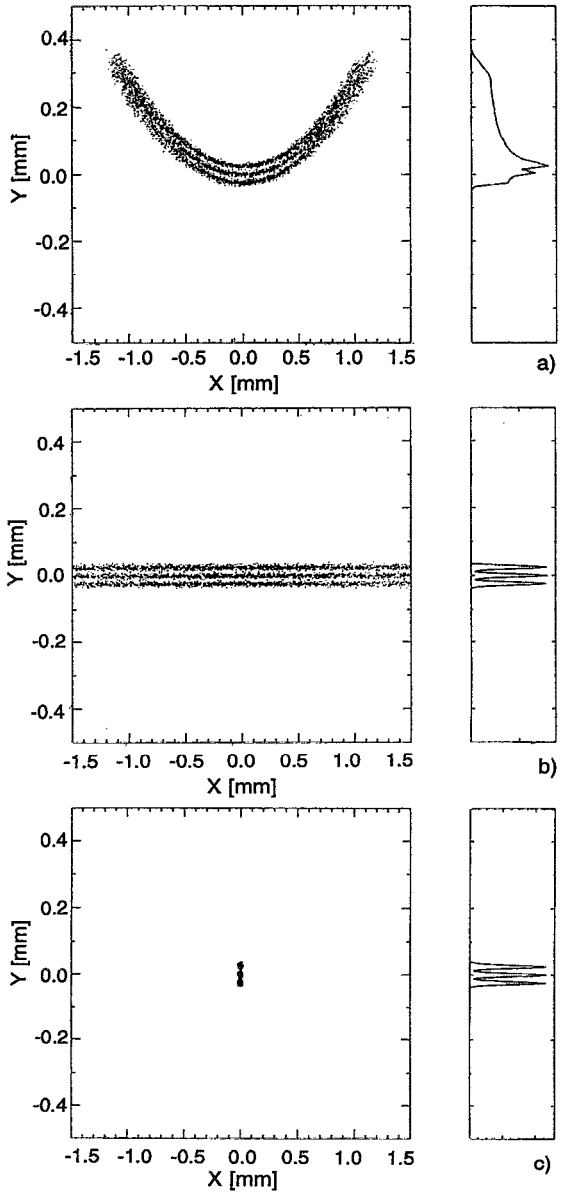

FIG. 9. Images of the light source in the plane of the exit slit, photon energies 399.9 eV, 400.0 eV, and 400.1 eV. Source size $\sigma_x = 300$ μm, $\sigma_y = 80$ μm, $r_1 = 15$ m, $r_3 = 1.5$ m, $c_{ff} = 2.25$. (a) Original design (Ref. 14), (b) Nyholms modification (Ref. 37), sagitally focusing mirror 3.8 m from the source. (c) Similar to (b), but sagitally focusing mirror close to the exit slit (distance 500 mm).

grating and virtual-source to grating were equal. With the rotationally symmetric ellipsoidal mirror the monochromator is then stigmatic [Fig. 3(d)]. Jark suggested using the ellipsoid in p reflection in order to reduce the effect of tangent errors.[41] That stigmatic beamline is in a commissioning state at the time of writing.

The aforementioned technological difficulty to manufacture aspheres of sufficiently high quality led to Padmore's proposal to choose a spherical mirror instead of an ellipsoidal one for focusing[42] [see Fig. 3(e)]. A similar decision was made at Hasylab for the SX700 monochromator at a triple Doris-Bypass-Undulator[43] and at BESSY for the HE-PGM-3

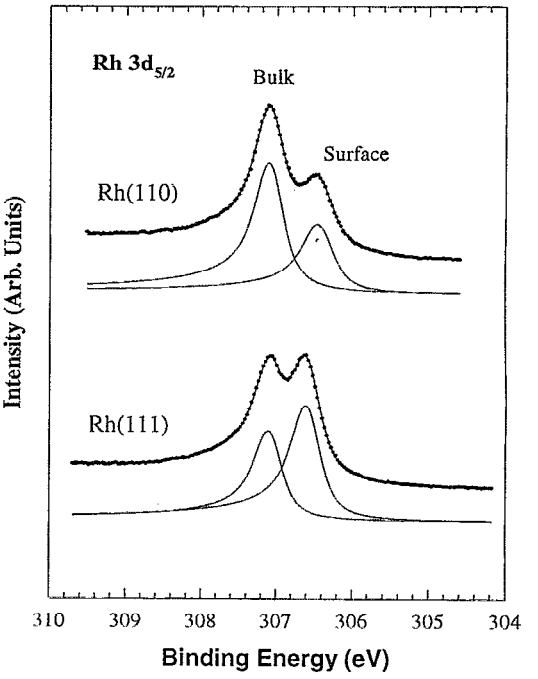

FIG. 10. Contributions from bulk and surface to the $3d_{5/2}$ electron energy distribution curve of the Rh(110) and the Rh(111) surface. The photon energy was 370 eV, the recording time 15 min for each spectrum (from Ref. 39).

at a dipole magnet.[44] One consequence was that the focal length had to be increased considerably in order to avoid excessive coma from the sphere (compare the raytracings in Fig. 11).

During commissioning of the SX700 at Hasylab[43] and

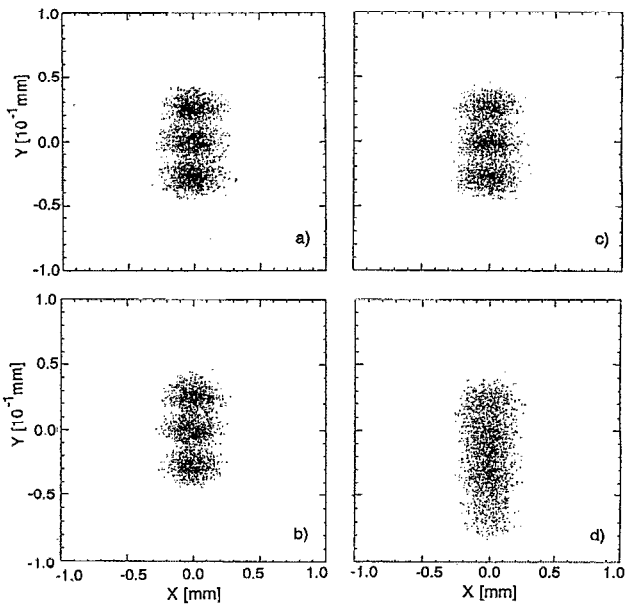

FIG. 11. Influence of coma when using a spherical focusing mirror: (a), (b) plane elliptical mirror, length 40 and 200 mm, (c), (d) spherical mirror, length 40 and 200 mm. Sagittal focusing is done in both cases with another plane elliptical mirror close to the exit slit.

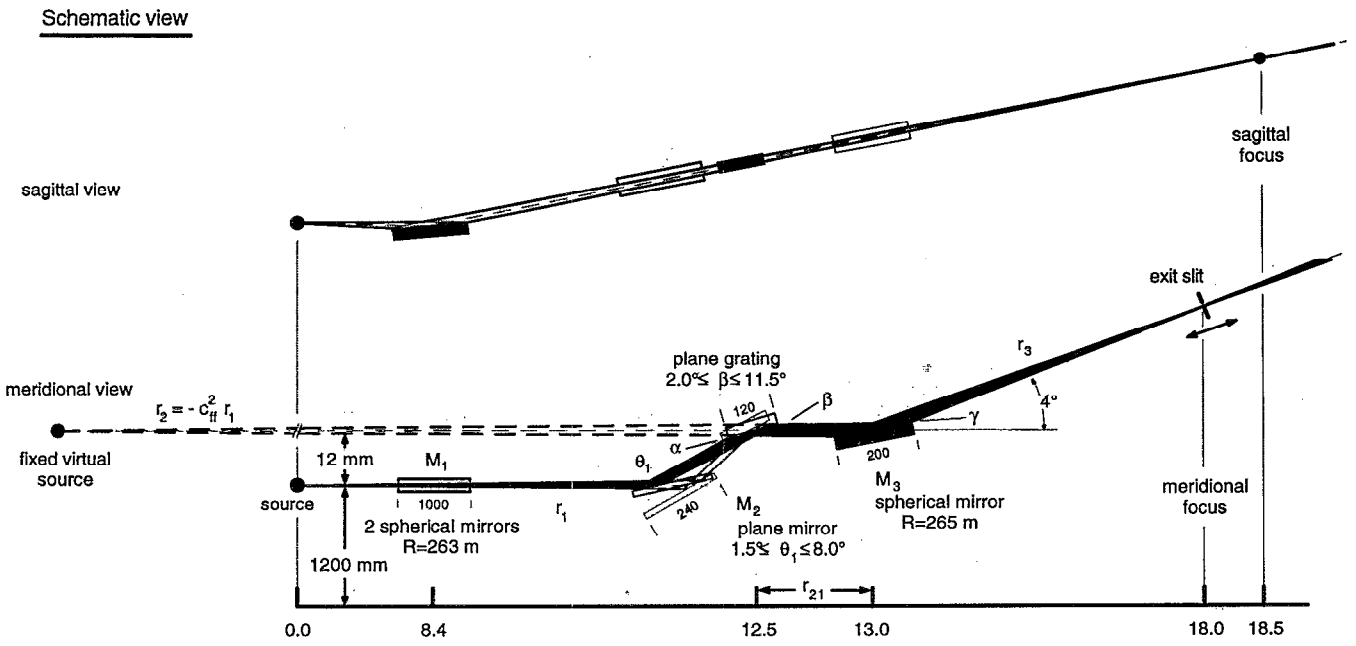

FIG. 12. Optical scheme of the HE-PGM-3. Note the 1 m long spherical premirror for sagittal focusing; the light comes from a dipole magnet.

the HE-PGM-3 at BESSY[10] in 1992, another interesting advantage inherent in the combination of the plane grating focusing condition and a spherical mirror was exploited: One can use different virtual source fix-focus constants c_{ff} for different purposes and still focus optimally after appropriate adjustment of the exit slit distance according to the equation

$$\frac{1}{r_2+r_{21}}+\frac{1}{r_3}=\frac{2}{R\sin\gamma}, \tag{7}$$

(see Fig. 12 for the parameters).

The standard value $c_{ff}=2.25$ was selected in 1980 on the basis of grating efficiency optimization over a broad photon energy range[14] (see Fig. 13). Values $c_{ff}<2.25$ give steeper angles for any given photon energy and do therefore decrease the higher order content. Values $c_{ff}>2.25$ give more grazing angles and higher spectral resolution because the virtual source distance increases with c_{ff}^2 and the virtual source size with c_{ff} which results in a stronger demagnification of the source into the plane of the exit slit. At the same time there is a certain decrease in flux because both the grat-

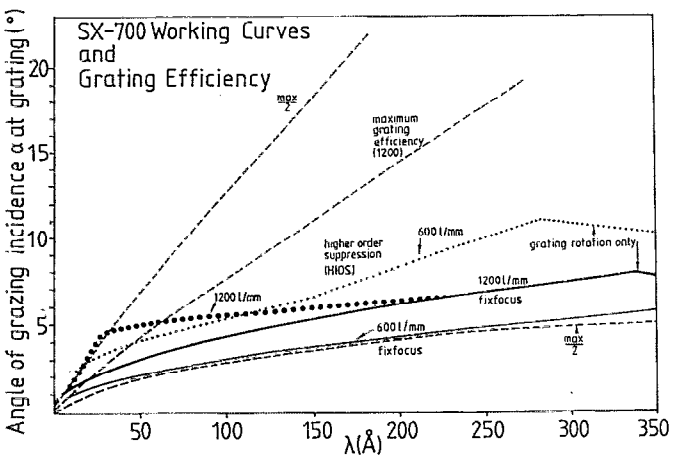

FIG. 13. On the grating efficiency map the $\alpha=f(\lambda)$-curve for maximum grating efficiency of a 1200 lines/mm grating is given together with the half-maximum curves for the more grazing and the more normal incident angle values (curves max/2). The working curves $\alpha=f(\lambda)$ of the SX700/1 for both gratings (1200 lines/mm, 600 lines/mm) and both modes of operation (fix focus and higher order suppression) are included (from Refs. 14 and 52).

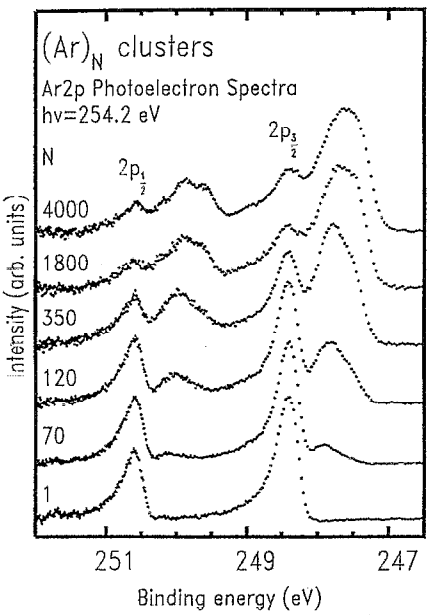

FIG. 14. A selection of argon $2p$ photoelectron spectra for argon clusters of various average sizes N (from Ref. 47).

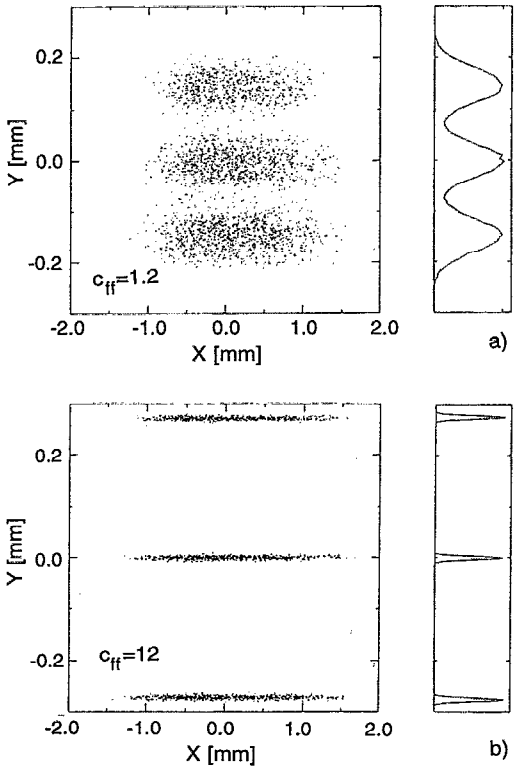

FIG. 15. HE-PGM-3 raytracing for $h\nu=400$ eV: (a) $c_{ff}=1.2$, (b) $c_{ff}=12$. The distance between the peaks is 500 meV and the source size is σ_x, $\sigma_y=300\ \mu\text{m}\cdot 100\ \mu\text{m}$ in both cases.

ing acceptance and grating efficiency go down. Note that the vertical beam size increases by a factor of c_{ff} at the grating in accordance with Liouville's theorem.

At Hasylab and at BESSY the result of the use of high c_{ff} values was very high spectral resolution immediately after installation of the high flux SX700[45,46] and the HE-PGM-3,[10] respectively. Figure 14 shows an example of research at the SX700 at Hasylab, the first energy resolved core level photoemission spectrum from clusters.[47]

To illustrate the nice optical trick of c_{ff} variation, we show in Fig. 15 ray tracings for two different cases: $c_{ff}=12$ and $c_{ff}=1.2$, all other parameters are unchanged. The system is obviously very flexible. The reader will probably agree that the effect is dramatic. It is twofold: The spatial width of the image decreases linearly with increasing c_{ff} and the energy width decreases more strongly than linearly because with increasing c_{ff} the grazing angle β goes down and therefore the dispersion $d\beta/d\lambda\sim 1/\sin\beta$ increases. Note that this is an optical advantage which does not exist in Rowland circle configurations: On the Rowland circle the ratio of the size of the entrance slit to its image at the exit slit is always 1:1.

In Table II we give some equations which should be useful for beamline designers. They describe the main features of monochromators applying the plane grating focusing condition: reciprocal dispersion, magnification, and coma from grating and sphere are given as a function of angles, fix-focus constant and beamline dimensions. The equations were deduced using the aberration term notations as given by

TABLE II. Grazing angles α, β at grating, reciprocal dispersion, magnification, and coma from grating and from spherical mirror as a function of wavelength and fix-focus constant c_{ff} for monochromators using the plane grating focusing condition:

Plane grating focusing equation: $\dfrac{\sin^2\alpha}{r_1}+\dfrac{\sin^2\beta}{r_2}=0$

Fix focus condition: $\dfrac{\sin\beta}{\sin\alpha}=\text{constant}=c_{ff}\Rightarrow r_2=-r_1\cdot c_{ff}^2=\text{constant}$

$$\alpha=\text{acos}\left[\frac{\lambda\cdot G}{c_{ff}^2-1}\cdot\left(\sqrt{c_{ff}^2+\frac{(c_{ff}^2-1)^2}{\lambda^2\cdot G^2}}-1\right)\right]$$

$$\beta=\text{asin}(c_{ff}\cdot\sin\alpha)$$

Reciprocal dispersion:

$$d\lambda/ds=\frac{\sin\beta}{n\cdot G\cdot r_3\cdot r_1\cdot\dfrac{c_{ff}^2}{r_1\cdot c_{ff}^2+r_{21}}}$$

for HE-PGM-3:

$$d\lambda/ds=\frac{\sin\alpha}{n\cdot 1221\cdot r_3\cdot 12500\cdot\dfrac{c_{ff}}{12500\cdot c_{ff}^2+500}}$$

Magnification:

$$Q=Q_{pg}\cdot Q_{fm}=\frac{r_2\cdot\sin\alpha}{r_1\cdot\sin\beta}\cdot\frac{r_3}{r_1\cdot c_{ff}^2+r_{21}}$$

for HE-PGM-3:

$$Q=\frac{c_{ff}\cdot r_3}{12500\cdot c_{ff}^2+500}$$

Coma (grating):

$$d\lambda_{cg}=\frac{1}{G}\cdot 1.5\cdot w_g^2\cdot\frac{\sin^2\alpha\cdot\cos\alpha}{r_1^2}+\frac{\sin^2\beta\cdot\cos\beta}{r_2^2}$$

for HE-PGM-3:

$$d\lambda_{cg}\sim=\frac{1}{G}\cdot 1.5\cdot w_g^2\cdot\alpha^2\cdot\frac{c_{ff}^2-1}{c_{ff}^2\cdot r_1^2}$$

Approximations: $\sin\alpha=\alpha$, $\cos\alpha=1-\dfrac{\alpha^2}{2}$, $\beta=c_{ff}\cdot\alpha$

for HE-PGM-3 typical value: $d\lambda_{cg}=\lambda\cdot 10^{-6}$

Coma (sphere):

$$ds_{cs}=r_3\cdot 1.5\cdot w_s^2\cdot\sin\gamma\cdot\cos\gamma\cdot\left[\frac{1}{(c_{ff}^2\cdot r_1+r_{21})^2}-\frac{1}{r_3^2}\right]$$

$$d\lambda_{cs}=d\lambda/ds\cdot ds_{cs}$$

for HE-PGM-3:

$$ds_{cs}=5000\cdot 1.5\cdot w_s^2\cdot\sin 2^\circ\cdot\cos 2^\circ\cdot\left[\frac{1}{(12500\cdot c_{ff}^2+500)^2}-\frac{1}{r_3^2}\right]$$

with:

G=grating ruling density,
n=spectral order,
w_g=half width of grating,
w_s=half width of spherical focusing mirror,
α=grazing angle "in" at grating,
β=grazing angle "out" at grating,
γ=grazing angle at spherical focusing mirror,
c_{ff}=fix focus constant,
r_1=distance source→plane grating,
r_2=distance grating→virtual source,
r_{21}=distance grating→focusing mirror,
r_3=distance focusing mirror→exit slit,
Q_{pg}=magnification by plane grating,
Q_{fm}=demagnification by focusing mirror.

HE-PGM-3 parameters: $r_1=12500$ mm, $r_{21}=500$ mm, $r_3=5000$ (+100, −300) mm, $G=1221$ lines/mm, 366 lines/mm, $w_g\leqslant 57$ mm, $w_s\leqslant 100$ mm, $\gamma=2^\circ$, compare Fig. 12.

TABLE III. Characteristic data of HE-PGM-3.

Grating 1221 lines/mm c_{ff}	r_3 (mm)	α (deg)	β (deg)	$\Delta h\nu/\Delta s$ (meV/μm)	Demagnification	Image of 300 μm source (meV FWHM)
Photon energy=100.0 eV						
1.60	5391.27	7.9386	12.7666	0.27496	3.7677	21.894
2.25	4985.65	4.9244	11.1362	0.25790	5.6858	13.607
5.00	4693.52	2.0271	10.1870	0.24929	13.3375	5.607
10.00	4641.35	0.9982	10.0326	0.24801	26.9426	2.762
Photon energy=280.0 eV						
1.60	5391.27	4.7609	7.6313	1.29562	3.7677	103.164
2.25	4985.65	2.9513	6.6524	1.21289	5.6858	63.996
5.00	4693.52	1.2143	6.0827	1.17111	13.3375	26.342
10.00	4641.35	0.5981	5.9915	1.16519	26.9426	12.974
Photon energy=400.0 eV						
1.60	5391.27	3.9856	6.3850	2.21429	3.7677	176.313
2.25	4985.65	2.4704	5.5654	2.07221	5.6858	109.337
5.00	4693.52	1.0164	5.0887	2.00058	13.3375	44.999
10.00	4641.35	0.5009	5.0148	1.99141	26.9426	22.174
Photon energy=530.0 eV						
1.60	5391.27	3.4635	5.5469	3.37889	3.7677	269.044
2.25	4985.65	2.1467	4.8346	3.16156	5.6858	166.815
5.00	4693.52	0.8834	4.4211	3.05247	13.3375	68.659
10.00	4641.35	0.4348	4.3518	3.03485	26.9426	33.792
Photon energy=1000.0 eV						
1.60	5391.27	2.5228	4.0386	8.76429	3.7677	697.855
2.25	4985.65	1.5635	3.5196	8.19833	5.6858	432.571
5.00	4693.52	0.6435	3.2189	7.91566	13.3375	178.046
10.00	4641.35	0.3165	3.1668	7.86563	26.9426	87.582
Photon energy=2000.0 eV						
1.60	5391.27	1.7843	2.8556	24.79903	3.7677	1974.619
2.25	4985.65	1.1059	2.4889	23.19689	5.6858	1223.945
5.00	4693.52	0.4554	2.2777	22.41020	13.3375	504.071
10.00	4641.35	0.2238	2.2387	22.24743	26.9426	247.720

Noda *et al.*,[48] and the case of a spherical focusing mirror has been selected.

Table III gives numerical values of the grazing angles at the grating, the reciprocal dispersion and the demagnification of the system as a function of both photon energy and fix-focus constant. The case of BESSY HE-PGM-3 is selected, which is described in more detail in the following section.

The HE-PGM-3

As mentioned above, at BESSY we decided in 1990 to build another PGM using the plane grating focusing condition and a spherical focusing mirror in that instrument for the same reasons as the SRC Daresbury and Hasylab had done earlier.[42,43] We employed a sagittally focusing premirror accepting 4 mrad horizontally from its dipole source (see Fig. 12). The exit slit is movable over a range of 4.7 m$<r_3<$5.1 m, and allows for c_{ff} values between 10.0 and 2.25.

The beamline was completed in November 1992 and first spectra were taken. Figure 16 shows flux data for the 1221 lines/mm grating obtained with a GaAs photodiode using the 200 μm exit slit and $c_{ff}=4.77$, the highest c_{ff} value we were able to reach during commissioning. With this grating the spectral range extends from 130 to ~2000 eV for $c_{ff}=2.25$ and from 108 to ~2000 eV for $c_{ff}=4.77$. The second grating has 366 lines/mm, the range extends from 40 to 850 eV with $c_{ff}=2.25$ and from 34 to 700 eV with $c_{ff}=4.77$.

The first flux data taken at the HE-PGM-3 showed deep minima at the carbon K edge and at the oxygen K edge,

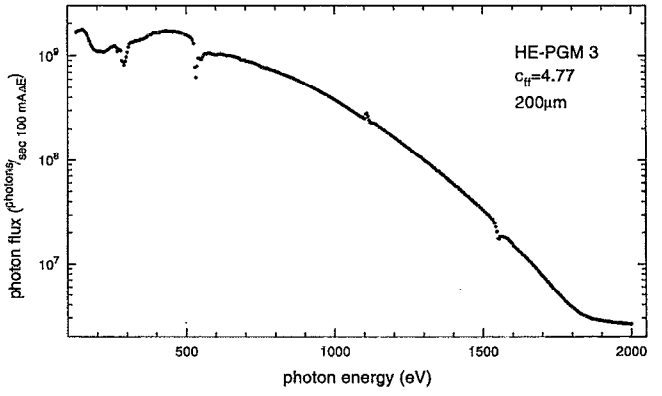

FIG. 16. Photon flux at the HE-PGM-3 using the 1221 lines/mm grating, $c_{ff}=4.77$, 2 mrad horizontally and the 200 μm exit slit. A GaAs photodiode was used. The Ga $L_{2,3}$ edge at 1116 eV is not completely normalized out.

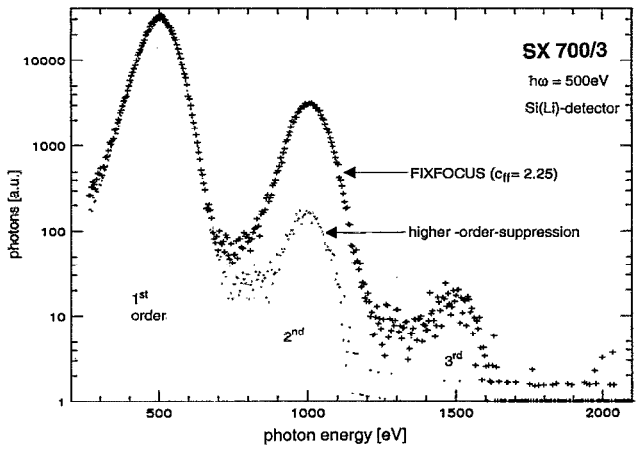

FIG. 17. Photons in first, second, and third order for $h\nu=500$ eV at the SX700/3. Data are shown for both the high resolution (FIXFOCUS) using $c_{ff}=2.25$ and the higher order suppression operational mode of the instrument. The intrinsic resolution of the Si(Li) detector is about 120 eV. Note the logarithmic scale (from Ref. 51).

indicating strong contamination of the optical elements. We therefore decided to perform an *in situ* HF-plasma cleaning of the optics.[49] The curve in Fig. 16 shows the flux after cleaning. The O_2 K minimum is still deep, and there is also a minimum at the Al K edge. We suspect that both minima come from Al_2O_3, aluminum has been used as a binding layer below the Au coating of the spherical mirrors.

At low photon energies and, in particular, when the 366 lines/mm grating is used, there is a considerable amount of higher order light in the spectra. A large part of the GaAs photodiode current then originates from photons in higher spectral orders, the quantum yield of the GaAs photodiode increases strongly with the photon energy.[50] At photon energies above ~400 eV, where energy dispersive Si(Li) detectors can be used, it is possible to separate these orders and an example of such measurements is shown in Fig. 17.[51] At low photon energies like 40 eV, the higher order content with

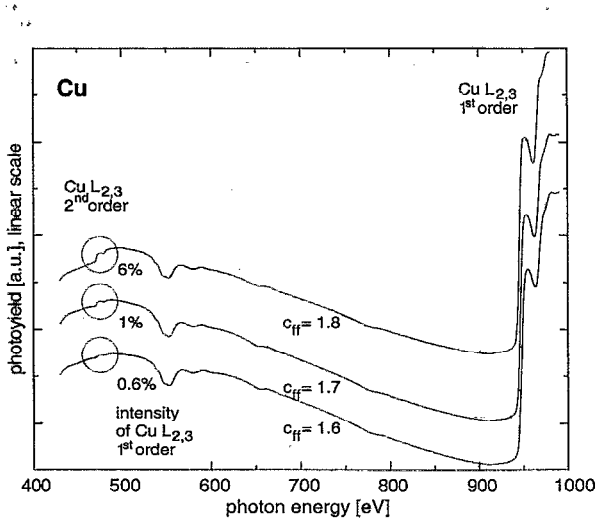

FIG. 18. Photoyield spectra of clean Cu for three different values of $c_{ff}=1.8$, 1.7, 1.6, showing the increasing spectral purity with decreasing c_{ff}, monochromator SX700/1 (Ref. 54).

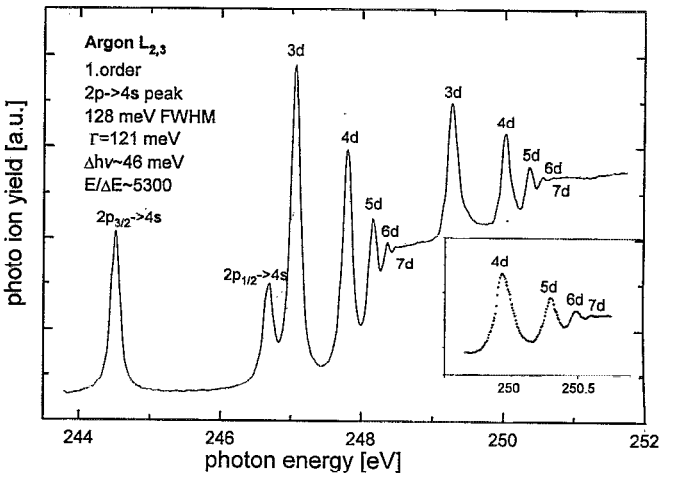

FIG. 19. Argon $L_{2,3}$ photo-ion-yield spectrum taken at the HE-PGM-3, first spectral order, small source size.

$c_{ff}\geqslant=2.25$ is clearly more than 10%. A special higher order supression mode was employed, which works at quite large grazing angles for any given wavelength in order to efficiently cutoff half that wavelength; then there is, of course, some loss in flux and spectral resolution.[52] About the same effect can be obtained with low c_{ff} values like $c_{ff}=1.6$[53] and in that case there is exact focusing onto a fixed exit slit at the same time. As an example Fig. 18 shows three photoyield spectra of clean Cu using $c_{ff}=1.8$, 1.7, 1.6. The intensity of the Cu $L_{2,3}$ edge in second order reaches values as low as 6‰ of the first order intensity.[54]

For a first estimate of spectral resolution we used a LaAl—sample which has a sharp $3d_{5/2}\rightarrow 4f$ resonance at 836 eV with a lifetime width of 730 meV.[55] With $c_{ff}=2.25$ and 20% of the vertical aperture 1.3 eV FWHM was achieved and the use of $c_{ff}=4.77$, second order light and a 10 μm exit slit reduced the measured FWHM to 0.78 eV. Simple quadratic subtraction of the lifetime width gives $\Delta h\nu\sim 0.27$ eV spectral resolution at 836 eV photon energy or $E/\Delta E>3000$.

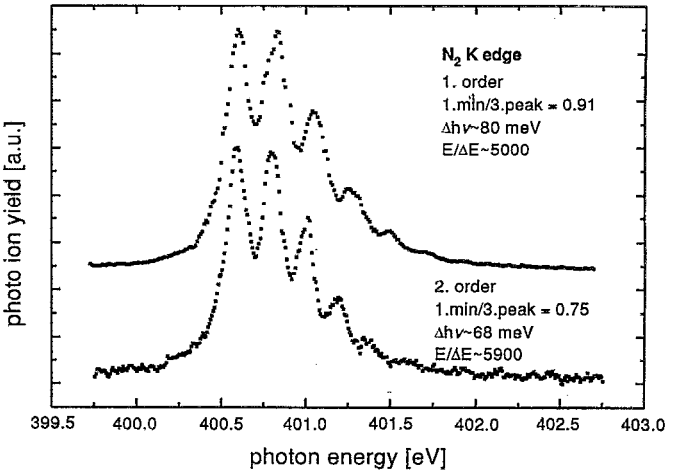

FIG. 20. N_2 K-photo ion yield spectrum taken at the HE-PGM-3, first spectral order, normal source size (a) and second order, small source size (b).

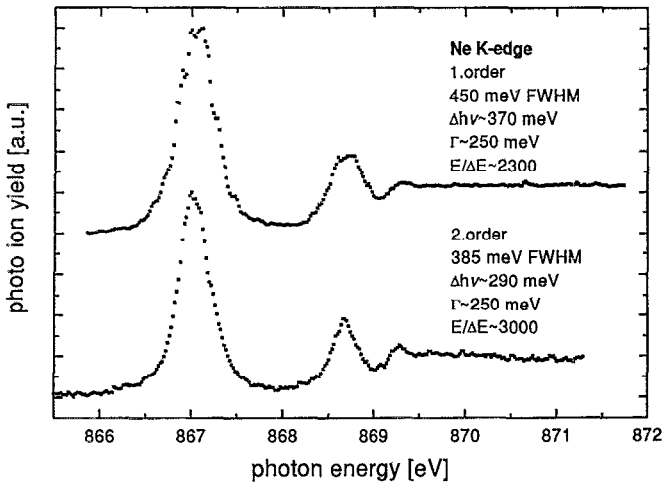

FIG. 21. Neon K-photon ion yield spectrum taken at the HE-PGM-3, first and second order, normal source size.

In order to obtain more detailed information on the spectral resolution capability, gas ion yield data were taken on argon, nitrogen, and neon. Figures 19–21 show the data. In Ar we find one more member of the infinite number of Rydberg states than hitherto reported. In N_2 we see the seventh vibrational level. The good statistics necessary for these observations are made possible through the availability of the full horizontal acceptance of 4 mrad during high resolution scans. The FWHM of the peaks and lifetime widths (Γ) from the literature are included.[55,56] In the case of Ne various values were deduced from previous experimental data: 310 meV,[57] 230 meV,[58] 215 meV.[13] In the presence of spectra with 290 meV FWHM,[13] the first value can now clearly be excluded; our smallest value was 338 meV FWHM measured with second spectral order and small source size. We used Γ=250 meV and simple quadratic subtraction to find an estimate of 370 meV (first order) and 290 meV (second order) for spectral resolution $\Delta h\nu$ at 867 eV photon energy and with the normal BESSY source size.

Fitting the data, especially in the case of N_2, proved to be not very satisfactory in the past and no consistent picture concerning the deduction of monochromator resolution from different sets of N_2 data arose. Although the 40 meV extracted by Chen and Sette[5] from their first high resolution

TABLE IV. Ratio of first minimum to third peak in the nitrogen $1s\rightarrow 1\pi_g^*$ spectra taken at various high resolution soft x-ray monochromators.

Monochromator	References	1. minimum/3. peak
(a) at dipole magnet beamlines:		
Dragon-SGM at NSLS	73	0.85
FU-SX700/2-PGM at BESSY	11	1.01 and 0.85 (2nd order)
UC/NL-SGM at SSRL	8	0.74
10 m GIM at photon factory	9	0.99
HE-PGM-3 at BESSY	(This work)	0.91 and 0.75 (2nd order)
(b) at insertion device beamlines:		
LBL-SGM at SSRL	6	0.93
X1B-SGM at NSLS	7	0.73
SX700-PGM at Hasylab	13	0.73 and 0.70 (2nd order)

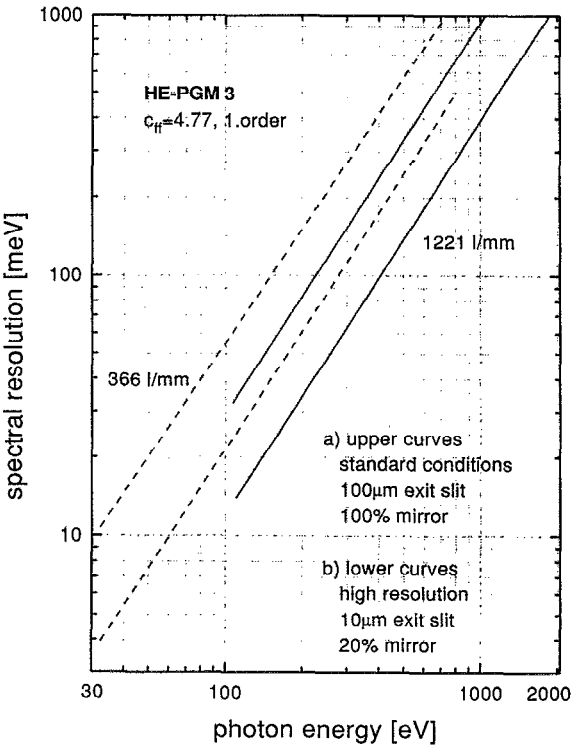

FIG. 22. Spectral resolution $\Delta h\nu$ as a function of $h\nu$ at the HE-PGM-3.

soft x-ray nitrogen data cannot necessarily be accepted as a definitive value, these authors propose useful criteria for determining the comparative resolution of soft x-ray monochromators as pointed out by Randall *et al.*[7] They take the first valley to third peak ratio in the N $1s\rightarrow\Pi_g^*$ absorption spectrum of N_2. As far as their resolution capability is concerned, various types of soft x-ray monochromators are quite close together, as the list of those ratios in Table IV illustrates.

Another helpful criterion to determine consistent resolution data for the HE-PGM-3 is the analytical functional dependence of the spectral resolution on photon energy: $dh\nu\sim h\nu^{3/2}$, which is valid for monochromators using the

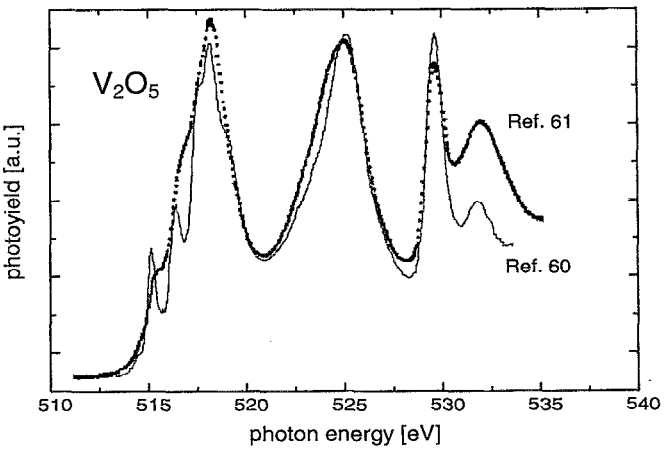

FIG. 23. Photoyield spectra of V_2O_5 taken at the HE-PGM-3 (from Ref. 60). A spectrum taken at a NSLS-SGM is included (Ref. 61). In both cases V_2O_5 single crystals were used.

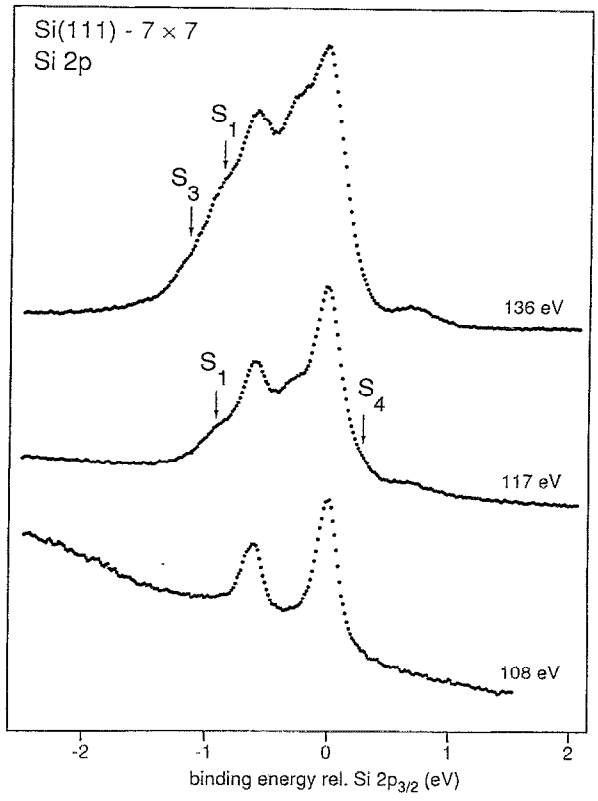

FIG. 24. Energy distribution curves of Si(111) 7×7 surface reconstruction at different photon energies as indicated (from Ref. 62). The bottom curve shows the bulk contribution of the spin orbit split Si $2p$ doublet. For the upper curves, arrows indicate features which are enhanced with increasing surface sensitivity.

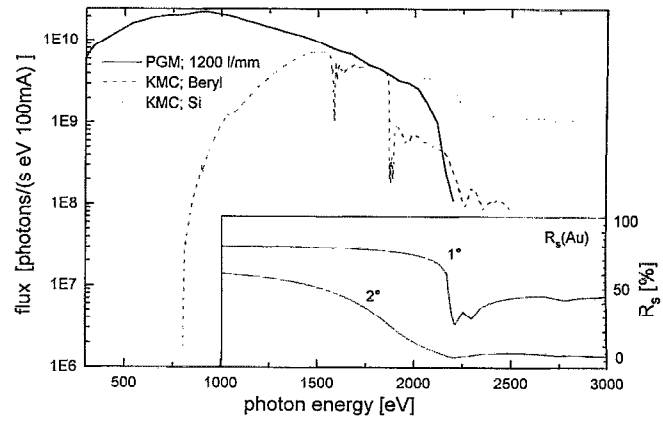

FIG. 25. Photon flux from a BESSY-PGM (here SX700/1) using a 1200 lines/mm grating and from the BESSY crystal monochromator KMC using beryl and Si crystals. Included are Au reflectivities R_s for grazing angles 1° and 2°.

plane grating focusing condition.[59] This relation has always been experimentally confirmed during the last ten years. Making use of the available experimental data and theoretical relations and conditions, we find the $\Delta h\nu(h\nu)$-lines given in Fig. 22. Note, that these PGMs are in focus at a fixed exit slit over the whole broad spectral range they cover. This is achieved with a single grating and is very different from other types of monochromators.

The HE-PGM-3 has, however, not been built for gas phase measurements but as a high resolution and high flux line primarily for photoemission and x-ray absorption experiments on solids and surfaces. First, such data were taken from February 1993 on. As an example we present the result of high resolution electron yield spectroscopy measurements on V_2O_5 single crystals cleaved under vacuum. Figure 23 shows the absorption in the region of the vanadium $L_{2,3}$ and the oxygen K edge. For the vanadium L_3 edge five features are resolved which reflect the projected density-of-states of the corresponding d orbitals.[60] For comparison, V_2O_5 single-crystal data taken some years ago at an NSLS-SGM are included in Fig. 23.[61] Using a high energy resolution hemispherical electron energy analyzer core level photoelectron spectroscopy experiments were carried out to study the Si(111)-7×7 reconstruction. At 10 μm exit slit width, fix-focus constant of 4.77 and 1 eV analyzer pass energy an overall instrumental energy resolution of 40–60 meV was achieved for photon energies between 108 and 190 eV. A representative set of spectra of the Si $2p$ line is shown in Fig. 24. Besides the Si $2p_{3/2,1/2}$ doublet from the bulk silicon (bottom trace in Fig. 24) and the well-known surface-related features S1 (rest atoms and atoms bound to adatoms) and S2 (adatoms) two new surface-related structures S3 and S4 are observed, which are attributed to the excitation of Si atoms in dimer rows and within the layer of Si atoms below the rest atoms, respectively.[62]

III. FURTHER CONSIDERATIONS

With the optical and technological developments of the last decade, grating instrumentation also did start to become attractive for research using photon energies above 1 keV, where they have, of course, to compete with crystal monochromators (for reviews see, e.g., Refs. 63 and 64). At BESSY, some work has also been done on crystal monochromator development and one goal was to extend their useful range to low photon energies. In Fig. 25 we show a comparison of flux data for a typical BESSY PGM and the crystal monochromator KMC using beryl and Si crystals.[65] Above 2 keV, where Si crystals can be used, crystal monochromators are superior. To really efficiently cover the 1–2 keV range with gratings one would have to go to grazing angles of 1° to obtain higher intensity. In the HE-PGM-3 case, for example, an intensity increase of a factor of ~20 at 2000 eV photon energy would occur when going from 2° to 1° at the sagittal and the meridional spherical focusing mirror, (compare the included curves). Another sometimes important point: grating monochromator flux spectra—with all optical elements being gold coated—are clearly smoother than those from crystal monochromators. Also concerning spectral resolution, gratings are competitive: with crystal monochromators using beryl crystals the achieveable spectral resolution at 1000 eV photon energy is about 0.5 eV as deduced from rocking curve measurements and parallel light[65] and about 0.8 eV as deduced from experimental data.[66] For grating monochroma-

tors values between 0.4 eV at 1000 eV and 1.1 eV at 2000 eV photon energy in first spectral order corresponds to the data presented in this paper.

The development of grating monochromators during the last 15 years has really been dramatic: In 1978 the first soft x-ray N_2 K spectra did not show any vibrational splitting at all, and were still considered very interesting at that time.[67]

At BESSY we are presently taking another step by combining the plane grating focusing condition for focusing and the technology of variable line spacing for spherical mirror coma compensation.[68] Such gratings should become available for instrumentation at our BESSY II storage ring presently under construction.

ACKNOWLEDGMENTS

We are grateful to F. C. Brown, C. T. Chen, L.-J. Lu, R. Nyholm, and H.-A. Padmore for their permission to reproduce optical schemes from their publications. We thank M. denBoer, M. Domke, F. de Groot, K. Horn, S. Horn, and R. Nyholm for making their experimental data available to us, partly prior to publication. The ionization chamber used was kindly loaned to BESSY by C. Kunz.

[1] See, e.g., Proc. XAFS V Conference, Seattle 1988, edited by J. M. deLeon, E. A. Stern, D. E. Sayre, Y. Ma, and J. J. Rehr, Physica B **158** (1989); Proc. XAFS VI Conf., York 1990, edited by S. S. Hasnain, *X-ray absorption fine structure* (Ellis Horwood, New York, 1991); Proc. XAFS VII Conf., Kobe 1992, edited by H. Kuroda, T. Ohta, T. Morata, Y. Udagawa, and M. Nomura, Appl. Phys. **32**, Suppl. 32-2 (1993); Proc. VUV 10 Conf., Paris 1992, edited by F. J. Wuilleumier, Y. Petroff, and I. Nenner (World Scientific, Singapore, 1993).

[2] For a list of SR facilities see: I. H. Munro, C. A. Boardman, and J. C. Fuggle, World Compendium of Synchrotron Radiation Facilities, The European Synchrotron Radiation Society, ISBN 9090042733.

[3] See, e.g., Proc. Int. Conf. X-ray and VUV Synchrotron Radiation Instrumentation (SRI), Stanford 1985, edited by G. S. Brown and I. Lindau, Nucl. Instrum. Methods Phys. Res. A **246** (1986); Proc. 6th Natl. Conf. SRI, Berkeley 1989, edited by R. C. C. Perera and A. C. Thompson, Nucl. Instrum. Methods Phys. Res. A **291** (1990); Proc. SRI III Conf., Tsukuba 1988, Rev. Sci. Instrum. **60** (1989); Proc. SRI IV Conf., Chester 1991, edited by I. H. Munro and D. J. Thompson, Rev. Sci Instrum. **63** (1992).

[4] C. T. Chen, Nucl. Instrum. Methods A **256**, 595 (1987).

[5] C. T. Chen and F. Sette, Rev. Sci. Instrum. **60**, 1616 (1989).

[6] P. A. Heimann, F. Senf, W. McKinney, M. Howells, R. D. van Zee, L. J. Medhurst, T. Lauritzen, J. Chin, J. Meneghetti, W. Gath, H. Hogrefe, and D. A. Shirley, Phys. Scripta T **31**, 127 (1990).

[7] K. J. Randall, J. Feldhaus, W. Erlebach, A. M. Bradshaw, W. Eberhardt, Z. Xu, Y. Ma, and P. D. Johnson, Rev. Sci. Instrum. **63**, 1367 (1992).

[8] L. J. Terminello, G. D. Waddill, and J. G. Tobin, Nucl. Instrum. Methods Phys. Res. A **319**, 271 (1992).

[9] A. Yagishita, S. Masui, T. Toyoshima, H. Maezawa, and E. Shigemasa, Rev. Sci. Instrum. **63**, 1351 (1992).

[10] W. B. Peatman, J. Bahrdt, A. Gaupp, F. Schäfers, and F. Senf, BESSY Annual Report 1992, p. 499 (unpublished).

[11] M. Domke, T. Mandel, A. Puschmann, C. Xue, D. A. Shirley, G. Kaindl, H. Petersen, and P. Kuske, Rev. Sci. Instrum. **63**, 80 (1992).

[12] H. Petersen, C. Jung, C. Hellwig, W. Peatman, and W. Gudat, BESSY Annual Report 1992, p. 494 (unpublished).

[13] C. U. S. Larsson, A. Beutler, O. Bjoerneholm, F. Federmann, U. Hahn, A. Rieck, S. Verbin, and T. Moeller, Nucl. Instrum. Methods Phys. Res. A **337**, 603 (1994).

[14] H. Petersen, BESSY Technical Report TB29 (1980) (unpublished); Opt. Commun. **40**, 402 (1982).

[15] H. A. Rowland, Am. J. Sci. **3**, 26 (1883).

[16] F. C. Brown, R. Z. Bachrach, and N. Lien, Nucl. Instrum. Methods **152**, 73 (1978).

[17] H. Ebert, Wied. Ann. **38**, 489 (1889).

[18] W. G. Fastie, J. Opt. Soc. Am. **42**, 641 (1952); and **42**, 647 (1952).

[19] M. Czerny and A. F. Turner, Z. Physik **61**, 792 (1930).

[20] C. Kunz, R. Haensel, and B. Sonntag, J. Opt. Soc. Am. **58**, 1415 (1968).

[21] A. H. C. P. Gilliesson, J. Sci. Instrum. **26**, 335 (1949).

[22] M. V. R. K. Murty, J. Opt. Soc. Am. **52**, 768 (1962).

[23] H. Dietrich and C. Kunz, Rev. Sci. Instrum. **43**, 434 (1972).

[24] F. Riemer and R. Torge, Nucl. Instrum. Methods **208**, 315 (1983).

[25] A. V. Pimpale, S. K. Deshpande, and V. G. Bhide, Appl. Opt. **30**, 1591 (1991).

[26] H. Petersen, J. Haase, A. Puschmann, A. Reimer, and R. Treichler, Ann. Israel Phys. Soc. **6**, 57 (1983).

[27] W. Peatman, Nucl. Instrum. Methods **222**, 6 (1984).

[28] H. Petersen, Nucl. Instrum. Methods Phys. Res. A **246**, 260 (1986).

[29] B. L. Henke, J. P. Knauer, and K. Premaratne, J. Appl. Phys. **52**, 1509 (1981).

[30] G. Kaindl, M. Domke, C. Laubschat, E. Weschke, and C. Xue, Rev. Sci. Instrum. **63**, 1234 (1992).

[31] M. Domke, G. Remmers, and G. Kaindl, Phys. Rev. Lett. **69**, 1171 (1992).

[32] H. Petersen, M. Willmann, F. Schäfers, and W. Gudat, Nucl. Instrum. Methods Phys. Res. A **333**, 594 (1993).

[33] A. Gaupp and M. Mast, Rev. Sci. Instrum. **60**, 2213 (1989).

[34] S. diFonzo, W. Jark, F. Schäfers, H. Petersen, A. Gaupp, and J. H. Underwood, Appl. Opt. **33**, 2624 (1994).

[35] L. Baumgarten, C. M. Schneider, H. Petersen, F. Schäfers, and J. Kirschner, Phys. Rev. Lett. **65**, 492 (1990).

[36] C. M. Schneider, K. Holldack, M. Kinzler, M. Grunze, H. P. Oepen, F. Schaefers, H. Petersen, K. Meinel, and J. Kirschner, Appl. Phys. Lett. **63**, 2432 (1993).

[37] R. Nyholm, S. Svensson, J. Nordgren, and A. Flodstroem, Nucl. Instrum. Methods A **246**, 267 (1986).

[38] See, e.g., A. Flodstroem, R. Nyholm, and B. Johannson, in *Synchrotron Radiation Research*, edited by R. Z. Bachrach (Plenum, New York, 1992), Vol. 1.

[39] J. N. Andersen, D. Heskett, E. Lundgren, M. Methfessel, R. Nyholm, and M. Scheffler, Phys. Rev. B (in press).

[40] L.-J. Lu and J.-Y. Chen, Nucl. Instrum. Methods Phys. Res. A **309**, 581 (1991).

[41] W. Jark, Rev. Sci. Instrum. **63**, 1241 (1992).

[42] H. A. Padmore, Rev. Sci. Instrum. **60**, 1608 (1989).

[43] R. Reininger and V. Saile, Nucl. Instrum. Methods Phys. Res. A **288**, 343 (1990).

[44] H. Petersen, W. Gudat, C. Hellwig, C. Jung, and W. Peatman, BESSY Annual Report 1991, p. 478 (unpublished).

[45] C. U. S. Larsson, F. Federman, A. Beutler, A. Rieck, S. Verbin, and T. Moeller, Hasylab Annual Report 1992, p. 100 (unpublished).

[46] T. Möller, Synchr. Rad. News **6**, 16 (1993).

[47] O. Björneholm, F. Federmann, F. Foessing, and T. Möller (unpublished).

[48] H. Noda, T. Namioka, and M. Seya, J. Opt. Soc. Am. **64**, 1031 (1974).

[49] M. Willmann, F. Eggenstein, W. B. Peatman, and H. Petersen BESSY Annual Report 1993, p. 467 (unpublished).

[50] M. Krumrey, E. Tegeler, J. Barth, M. Krisch, F. Schaefers, and R. Wolf, Appl. Opt. **27**, 4336 (1988).

[51] H. Petersen, W. Braun, M. Krumrey, E. Tegeler, A. Goldmann, F. Lodders, and D. Rudolph, Ital. Phys. Soc. Conf. Proc. **25**, 315 (1989).

[52] H. Petersen, SPIE Proc. **733**, 262 (1986).

[53] F. Scholze, M. Krumrey, P. Mueller, and D. Fuchs, Rev. Sci. Instrum. **65**, 3229 (1994).

[54] H. Wende and K. Baberschke (private communication).

[55] E. J. McGuire, Phys. Rev. A **5**, 1043 (1972).

[56] G. C. King, M. Tronc, F. H. Read, and R. C. Bradford, J. Phys. B **10**, 2479 (1977).

[57] A. P. Hitchcock and C. E. Brion, J. Phys. B **13**, 3269 (1980).

[58] U. Gelius, S. Svensson, H. Siegbahn, E. Baisilier, A. Faxaelv, and K. Siegbahn, Chem. Phys. Lett. **28**, 1 (1974).

[59] W. Braun, H. Petersen, J. Feldhaus, A. M. Bradshaw, E. Dietz, J. Haase, I. T. McGovern, A. Puschmann, A. Reimer, H. H. Rotermund, and R. Unwin, SPIE **447**, 117 (1984).

[60] O. Müller, E. Göring, M. L. denBoer, and S. Horn, BESSY Annual Report 1993 p. 333 (unpublished).

[61] F. M. F. de Groot, Thesis, Nijmegen University, 1991, see also: M. Abbate, H. Pen, M. T. Czyzyk, F. M. F. de Groot, J. C. Fuggle, Y. J. Ma, C. T. Chen, F. Sette, A. Fujimori, Y. Ueda, and K. Kosuge, J. Electron. Spec. Rel. Phen. **62**, 185 (1993).

[62] J. J. Paggel, W. Theis, K. Horn, C. Hellwig, Ch. Jung, and H. Petersen, Phys. Rev. B (in press).
[63] W. Gudat and C. Kunz, in *Synchrotron Radiation*, edited by C. Kunz, Topics in Current Physics (Springer, Heidelberg, 1978).
[64] T. Namioka and K. Ito, Phys. Scripta **37**, 673 (1988).
[65] J. Feldhaus, F. Schäfers, and W. Peatman, SPIE Proc. **733**, 242 (1986).
[66] S. W. Kortboyer, J. B. Goedkoop, F. M. F. de Groot, M. Grioni, J. C. Fuggle, and H. Petersen, Nucl. Instrum. Methods Phys. Res. A **275**, 435 (1989).
[67] A. Bianconi, H. Petersen, F. C. Brown, and R. Z. Bachrach, Phys. Rev. A **17**, 1907 (1978).
[68] H. Petersen and F. Senf, BESSY Annual Report 1993, p. 449 (unpublished).
[69] E. Morikawa, J. D. Scott, E. D. Poliakoff, R. L. Stockbauer, and V. Saile, Rev. Sci. Instrum. **63**, 1300 (1992).
[70] B. C. Craft, M. Feldmann, E. Morikawa, E. D. Poliakoff, V. Saile, J. D. Scott, and R. L. Stockbauer, Rev. Sci. Instrum. **63**, 1561 (1992).
[71] S. Aksela, A. Kivimaeki, R. Nyholm, and S. Svensson, Rev. Sci. Instrum. **63**, 1252 (1992).
[72] C. S. Mythen, G. v. d. Laan, and H. A. Padmore, Rev. Sci. Instrum. **63**, 1313 (1992).
[73] C. T. Chen, Y. Ma, and F. Sette, Phys. Rev. A **40**, 6737 (1989).